First publ. in: Langmuir 20 (2004), 18, pp. 7811-7819

Mixed Micellar Phases of Nonmiscible Surfactants: Mesoporous Silica with Bimodal Pore Size Distribution via the Nanocasting Process

Matthijs Groenewolt and Markus Antonietti*

Max Planck Institute of Colloids and Interfaces, Research Campus Golm, D-14424 Potsdam, Germany

Sebastian Polarz

Ruhr Universität Bochum, Chemistry Department, D-44780 Bochum, Germany

Highly organized mesoporous silica monoliths were reproducibly prepared by nanocasting mixtures of fluorinated nonionic surfactants and micelles of two hydrocarbon block copolymers. It is the special feature of this fluorocarbon/hydrocarbon template mixture that they form not mixed micelles but individual micelles instead. By careful analysis of the pore architectures by gas sorption measurements and transmission electron microscopy in dependence on the relative template concentration, two different situations could be identified: (a) mesoscopically demixed samples and (b) mixed micellar phases where the two different micelles are packed in some type of organized alloy phase. Besides identification of such mixed phases for the first time for fluorocarbon/hydrocarbon mixtures, the resulting porous systems with controlled bimodal pore size distribution might be interesting from a materials perspective.

Introduction

The synthesis of porous matter, omnipresent in nature for structural and functional reasons, has recently experienced enhanced interest in materials chemistry, for a number of reasons. This started from the observation that micelles and lyotropic phases can be used as templates to generate mesoporous silica with a variety of textures (the so-called MCM materials, see refs 1 and 2). Meanwhile, the range of organic supramolecular templates has been significantly extended (polymers, block copolymers, polysaccharides, cyclodextrines, and polymer latexes; for a review, see ref 3), and practically any pore size and pore architecture can be rationally accessed. The precision of the replication, especially in the so-called nanocasting process, is sometimes so high that one can even learn from the pore structure about the assembly structure of the template in it, as for instance delineated for the packing of spherical micelles[4] or the mutual arrangement of cyclodextrine moieties.[5]

A problem we regard as still interesting is the construction of materials with hierarchical or multimodal pore architectures. Here the big pore system accomplishes optimized transport, whereas the small pores provide the surface area and the size selectivity, without the possibility that the channel system can be efficiently blocked. The natural attempt to achieve bimodal pore size distributions in mesoporous silica is to use templates of different size which do not interfere with each other. This is rather simple when using rigid latex templates[6,7] but is demanding for soft self-organizing systems as such systems usually form mixed aggregates. In addition, latex templates are restricted toward smaller pore sizes to about 30−50 nm in size.

In this study, hydrocarbon block copolymer templates which are known to generate 9 and 13 nm large spherical pores, respectively, are mixed with a fluorinated hydrocarbon for simultaneous nanocasting. The fluorocarbon/hydrocarbon situation is known to form separated micelles even in complex mixtures,[8−10] as long as both surfactants have sufficient size. Since fluorinated porogens promise specific advantages (such as new, fluorocarbon-specific phase morphologies[11] or the potential for templating organically modified silica precursors), their usefulness was first investigated in the pure state.

By characterization of the samples with small-angle X-ray scattering (SAXS), nitrogen sorption, and transmission electron microscopy (TEM) analysis, we expect to reveal a quite detailed picture of structure formation and template compatibility.

Experimental Section

The fluorinated surfactants Fluowet OTN and Fluowet OTL (for structures, see Figure 1) were kind gifts from Clariant. The SE3030 polymer was obtained from Goldschmidt, and the KLE3935 polymer was synthesized by a procedure described elsewhere.[4] Tetramethoxysilane (TMOS) was purchased from Aldrich. All commercial chemicals have been used without further purification.

(1) Beck, J. S.; Vartuli, J. C.; Roth, W. J.; Leonowicz, M. E.; Kresge, C. T.; Schmitt, K. D.; Chu, C. T. W.; Olson, D. H.; Sheppard, E. W.; McCullen, S. B.; Higgins, J. B.; Schlenker, J. L. *J. Am. Chem. Soc.* **1992**, *114*, 10834−10843.

(2) Kresge, C. T.; Leonowicz, M. E.; Roth, W. J.; Vartuli, J. C.; Beck, J. S. *Nature* **1992**, *359*, 710−712.

(3) Polarz, S.; Antonietti, M. *Chem. Commun.* **2002**, 2593−2604.

(4) Thomas, A.; Schlaad, H.; Smarsly, B.; Antonietti, M. *Langmuir* **2003**, *19*, 4455−4459.

(5) Polarz, S.; Smarsly, B.; Bronstein, L. M.; Antonietti, M. *Angew. Chem., Int. Ed.* **2001**, *40*, 4417−4421.

(6) Antonietti, M.; Berton, B.; Göltner, C. G.; Hentze, H.-P. *Adv. Mater.* **1998**, *10*, 154−159.

(7) Zhou, Y.; Antonietti, M. *Chem. Commun.* **2003**, 2564−2565.

(8) Weberskirch, R.; Nuyken, O. *J. Macromol. Sci., Pure Appl. Chem.* **1999**, *A36*, 843−857.

(9) Stähler, K.; Selb, J.; Candau, F. *Langmuir* **1999**, *15*, 7565−7576.

(10) Barthelemy, P.; Tomao, V.; Selb, J.; Chaudier, Y.; Pucci, B. *Langmuir* **2002**, *18*, 2557−2563.

(11) Burger, C.; Micha, M.-A.; Oestreich, S.; Förster, S.; Antonietti, M. *Europhys. Lett.* **1998**, *42*, 425−429.

$CF_3[CF_2]_{6\text{-}16}C_2H_4\text{-}EO_{4\text{-}5}$ Fluowet OTN ™

$CF_3[CF_2]_{6\text{-}16}C_2H_4\text{-}EO_{7\text{-}8}$ Fluowet OTL ™

Figure 1. Formulas of the used fluorinated surfactant templates.

Preparation of the Porous Silica Materials Based on Pure Fluorinated Surfactant. In a typical synthesis, 0.30 g of fluorinated surfactant was dissolved in 1.0 g of TMOS. 0.5 g of a 0.01 M aqueous HCl solution was added, and the mixture was slightly heated and treated with ultrasound for 5 min. The homogenized mixture was exposed to a gentle vacuum to remove the methanol formed due to the hydrolysis of the TMOS. The homogeneous and highly viscous solution is poured into a Petri dish, and formation and conservation of the lyotropic phase are controlled during the condensation via a polarization microscope. After 24 h, the resulting hybrid material is calcined by heating the samples up to 550 °C with a temperature ramp of 5 K/min, followed by isothermal treatment at 550 °C for 4 h. The combustion gases were washed with concentrated $Ca(OH)_2$ solution in order to remove HF.

Preparation of the Porous Silica Materials Based on the Binary OTN−SE3030 Polymer System. SE3030 (0.12 g) was dissolved in 1.0 g of TMOS. After homogenization of the mixture, 0.5 g of a 0.01 M aqueous HCl solution was added, and the mixture was homogenized again using slightly elevated temperature and ultrasound.

The mixture was divided into appropriate portions (e.g., 0.30 g; contains 7.3% or 0.022 g of SE3030), and the required amount of fluorinated polymer (OTN) was added for the desired OTN/(SE3030 + OTN) ratio (e.g., 0.027 g to achieve a OTN/(SE3030 + OTN) ratio of 35%; sample SE-4). Again complete homogenization was achieved using slightly elevated temperature and ultrasound. The reaction mixtures were freed from methanol by a gentle vacuum and allowed to complete gelation overnight in a 1 mL open tube.

The resulting monolithic gels were calcined by the same procedure described above.

Preparation of the Porous Silica Materials Based on the Binary OTN−KLE3935 Polymer System. For the KLE3935 mixture, 0.33 g of KLE3935 was mixed with 3.3 g of a 1/1 mixture of TMOS/ethanol. After addition of 0.8 g of a 0.01 M aqueous HCl solution, the mixture was homogenized. A second mixture was prepared by dissolving 0.30 g of OTN in 1.0 g of TMOS. After adding 0.8 g of a 0.01 M aqueous HCl solution, the mixture was also homogenized.

These two solutions were mixed and homogenized to get the different OTN/KLE3935 ratios (e.g., 200 mg of KLE3935 solution (contains 7.5% or 0.015 g of polymer) and 20 mg of OTN solution (contains 14.3% or 0.003 g of polymer) give a polymer ratio of OTN/(KLE3935 + OTN) = 17%; sample KLE-1). Evaporation and calcination are carried out in the same manner as for the SE3030/OTN system.

Characterization of Mesoporous Materials. TEM images were taken using a Zeiss EM 912Ω at an acceleration voltage of 120 kV. Samples were ground in a ball mill and dispersed in acetone. One droplet of the suspension was applied to a 400 mesh carbon-coated copper grid and left to dry in air.

SAXS patterns were recorded employing a Kratky camera.

Nitrogen sorption data were obtained with a Micromeritics Tristar 3000.

Results

First, we analyzed the products of the nanocasting procedure for the pure fluorocarbon surfactant phases. For that, we employed two commercial, nonionic surfactants which differ only in the length of the hydrophilic oligo(ethylene oxide) moiety (see Figure 1).

The surfactants, in short OTN and OTL, were chosen due to their commercial availability and the fact that they show pronounced lyotropic phases with strong birefringence even in the precondensed reaction mixture, as illustrated by the two polarized optical microscopy (POM) pictures shown in Figure 2.

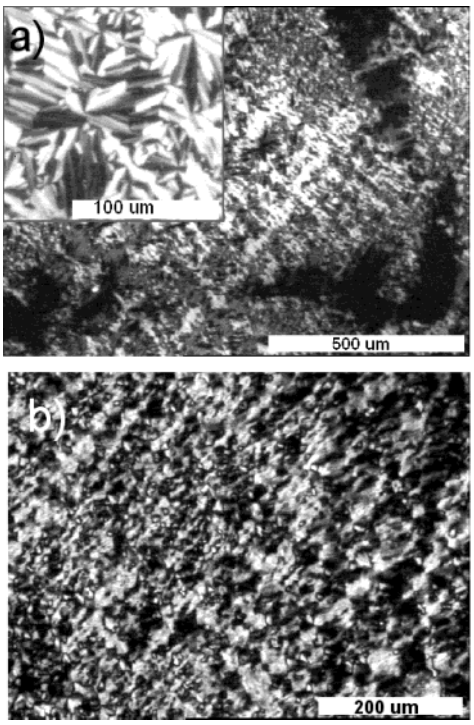

Figure 2. (a) POM image of the mesophase of sample OTN-3 prior to condensation and after evaporation of the alcohol, containing silicic acid. A hexagonal texture with extended domains can be identified, better seen in the inset. (b) POM image of sample OTL-2, under similar conditions. The domains are not as marked as for OTN, but the texture shows hexagonal features, too.

The high stability and pronounced formation of long range ordered phases even in the presence of the hydrolyzed silica precursor make both fluorinated surfactants good candidates as porogens. During the writing of this article, we found out that Blin et al. have proven this point by reporting the preparation of mesoporous hexagonal silica[12] using a nonionic fluorinated surfactant similar to our templates but employed a hydrothermal, SBA-like synthesis. In the Blin case, the surfactant/silica molar ratio was kept constant at 0.5, which corresponds to a template content of 88 wt % of the final condensed material. As our aim is the synthesis of a precise, monolithic replica of the lyotropic phase via the nanocasting route, we decided, without knowledge of the other work, to use much lower ratios of surfactant/silica.

The prepared samples were allowed to gel completely and were calcined afterward, while the amount of template was varied in a systematic fashion. The compositions under examination are summarized in Table 1.

In nanocasting, it is possible to replicate even dilute micellar phases, but materials templated in this way are usually hard to calcine, as the organic material can hardly leave the silica matrix and is partly transferred into carbon or black condensates. This is why a white, carbon-free monolith is usually a signature for the percolation of the template structures and formation of a continuous channel system.

Referring to Table 1 and judging by the color, percolation of the ethylene oxide (EO) brushes of the micelles within the silica starts at about 40 wt % polymer content, as

(12) Blin, J. L.; Lesieur, P.; Stebe, M. J. *Langmuir* **2004**, *20*, 491−498.

Table 1. Mesoporous Materials Synthesized with Different Ratios of Fluorinated Surfactants Relative to the Final Amount of SiO

sample code	OTN/g	OTL (40 wt %)/g	mL HCL, pH = 2	TMOS/g	SiO_2/g	wt % template in completely condensed material	POM texture	carbon-free after calcination?
OTN-1	0.25		1.3	2.56	1	20	no	no
OTN-2	0.50		1.3	2.56	1	33	weak	no
OTN-3	0.77		1.3	2.56	1	44	strong	yes
OTN-4	1.00		1.3	2.56	1	50	no	yes
OTL-1		1.23 (0.51)	0.7	2.56	1	34	weak	no
OTL-2		2.50 (1.00)	0.3	2.56	1	50	strong	yes
OTL-3		3.90 (1.56)	0.3	2.56	1	61	strong	yes

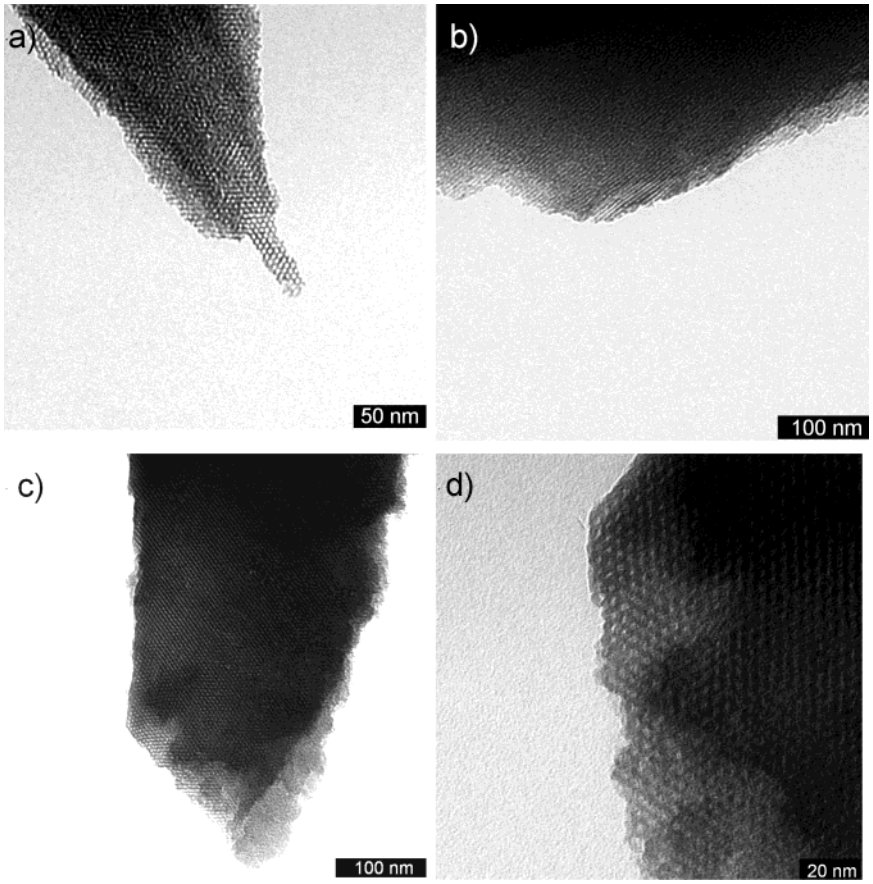

Figure 3. TEM pictures of OTN-3 (a,b) and OTL-2 (c,d). Both samples show nicely ordered hexagonal mesophases (a,c,d), as indicated by the silica replicas.

calculated for the completely condensed material (SiO_2). Both polymers do form a birefringent lyotropic phase in the present reaction system around a concentration of about 30−50 wt % related to silica.

The TEM pictures of the samples with strong polarization textures also show, for both surfactants, clearly well ordered domains with a hexagonal arrangement of the single pores, as depicted in Figure 3.

From the TEM pictures, the pore width is estimated to be around 2.6 (±0.3) nm for OTL and 2.8 (±0.5) nm for the OTN-based material.

The Brunauer−Emmett−Teller (BET) measurements of the synthesized materials (Figure 4) exhibit a typical adsorption isotherm for mesoporous materials, with relatively small micropore content. Capillary condensation takes place at reduced pressures of $P/P_0 < 0.4$, which is pointing to pores with an average pore width of about 3 nm. The difference of the position of the steepest slope, that is, where capillary condensation occurs, is slightly shifted toward higher relative pressures in the OTL-based material, which refers to bigger pores in this material. This is verified by density functional theory (DFT) calculations; that is, the pores in the OTN material are determined to be 2.7 nm, whereas the OTL material possesses 3.1 nm big pores. This is in good agreement with the TEM observations.

The fact that OTN- and OTL-based silicas have a slightly different pore size, although their hydrophobic part, for example, the fluorinated tail, is the same, was similarily found for nonionic hydrocarbon surfactants and was explained by the so-called three-phase model;[13] that is, parts of the hydrophilic tail also contribute to the mesopore volume.

All these results underline that the pure fluorinated surfactants are in general also nicely suited as porogens for silica; the two sets of data on the pure fluorosurfactants are however also relevant as a reference to judge the binary systems under discussion below.

(13) Smarsly, B.; Polarz, S.; Antonietti, M. *J. Phys. Chem. B* **2001**, *105*, 10473−10483.

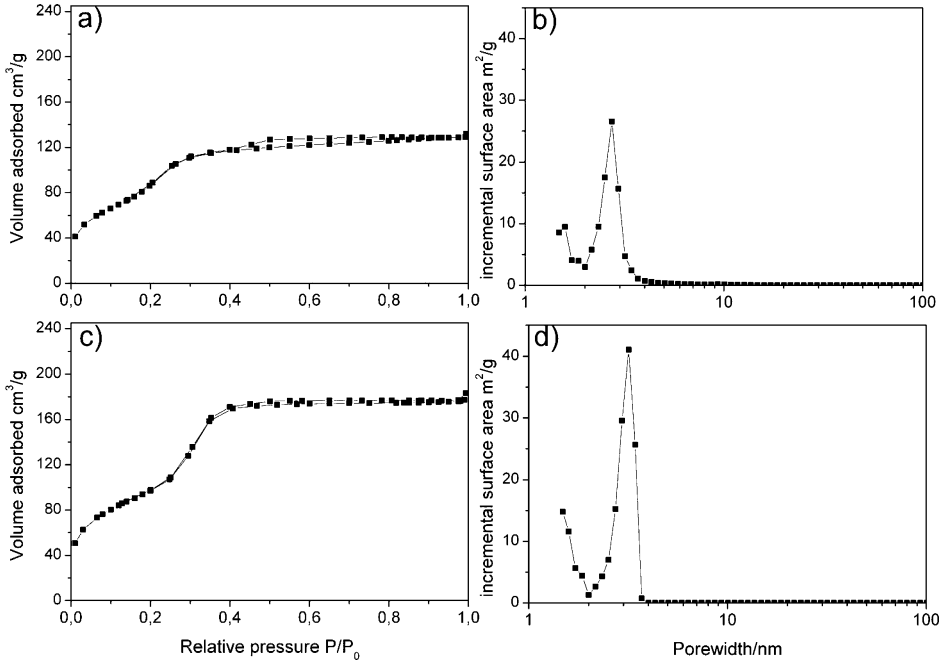

Figure 4. BET isotherm (a) and corresponding DFT calculation (b) for OTN-3. The DFT calculation shows a narrow pore size distribution with an average value of 2.7 nm. BET isotherm (c) and corresponding DFT calculation (d) for OTL-2. The DFT calculation shows a narrow pore size distribution with an average value of 3.1 nm.

Table 2. SE-Based Mixed Mesoporous Materials Synthesized with Different Ratios of OTN to SE3030, Increasing the Amount of Fluorocarbon Pores in Addition to the Hydrocarbon Pores

sample code	SE3030/g	OTN/g	% template giving small pores	HCl, pH = 2/g	TMOS/g	SiO_2/g	wt % template in completely condensed material
SE-1	0.30	0.03	9	1.25	2.56	1	25
SE-2	0.30	0.08	21	1.25	2.56	1	28
SE-3	0.30	0.18	37	1.25	2.56	1	32
SE-4	0.30	0.37	55	1.25	2.56	1	40
SE-5	0.30	0.69	70	1.25	2.56	1	50
SE-6	0.30	1.52	84	1.25	2.56	1	65

Binary Template Systems of Fluorinated Surfactants and Amphiphilic Hydrocarbon Block Copolymers

To simplify analysis and to ensure the absence of miscibility between fluorinated and hydrocarbon species, we decided to use two block copolymer templates with sufficient molecular weight whose phase behavior was already examined in previous publications.[4,14] SE3030 is a polystyrene-*b*-ethylene oxide block copolymer with a molecular weight of 3000 g/mol for each block, whereas KLE3935 is a hydrogenated polybutadiene-*b*-ethylene oxide block copolymer with molecular weights of 3935 g/mol (the KratonLiquid based hydrogenated polybutadiene) and 3460 g/mol (poly(ethylene oxide)).

Nanocasting of the SE3030/OTN System. Six different compositions of SE3030/OTN were used as templates in the standard procedure in order to get a bimodal pore size distribution. OTN was used, as OTL micelles and phases turned out to be too incompatible to reveal homogeneous systems. The compositions are summarized in Table 2. All samples turned out to be carbon-free after calcination, that is, exhibited an open pore structure.

The materials rich in block copolymer, SE-1 to SE-3, show the typical texture of the pure block copolymer (Figure 5). The samples look homogeneous, although macroscopically demixing into pure SE3030 and OTN micelles already starts for sample SE-3 at some spots of the sample.

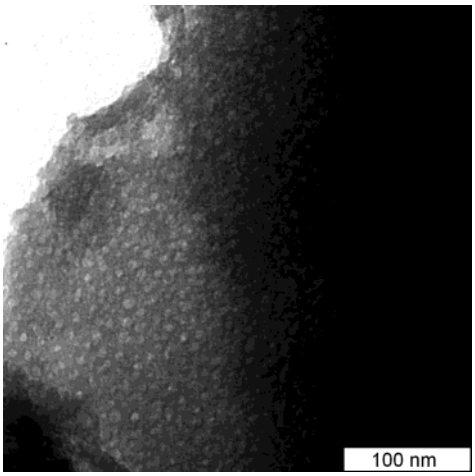

Figure 5. TEM picture of calcined SE-2. The typical SE structure is reproduced. The OTN pores are weakly detectable since their relative importance is low.

Figure 6 shows the adsorption/desorption isotherms of the synthesized materials SE-1 to SE-3. In comparison to the reference, which is the corresponding pure SE3030 silica with 10 wt % polymer template (with respect to the silica matrix), additional surface is created. Interestingly, the isotherms show no significant gain of microporosity with increasing concentration of OTN. The additional

(14) Göltner, C. G.; Henke, S.; Weissenberger, M.; Antonietti, M. *Angew. Chem., Int. Ed.* **1998**, *37*, 613−616.

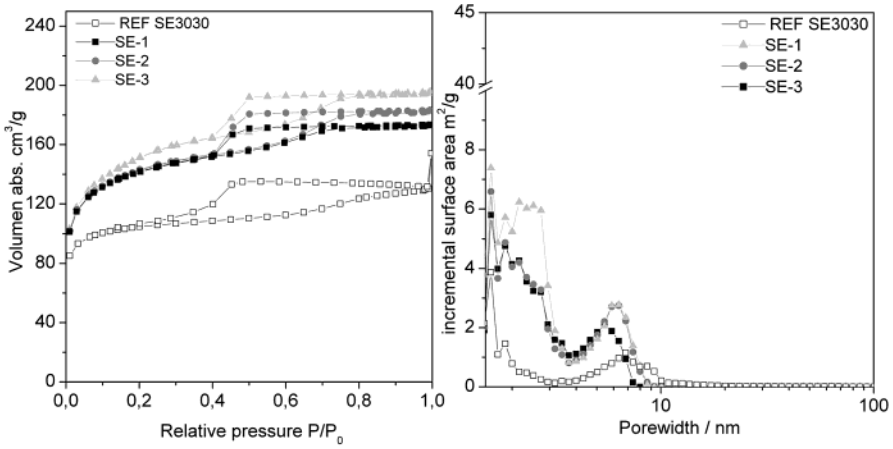

Figure 6. BET isotherms of the calcined materials SE-1 to SE-3. The DFT calculations for SE-1 and SE-2 are mainly sensitive to the pores generated by the SE3030 template. For SE-3, the smaller OTN pores can be numerically separated and show up in the pore size distribution.

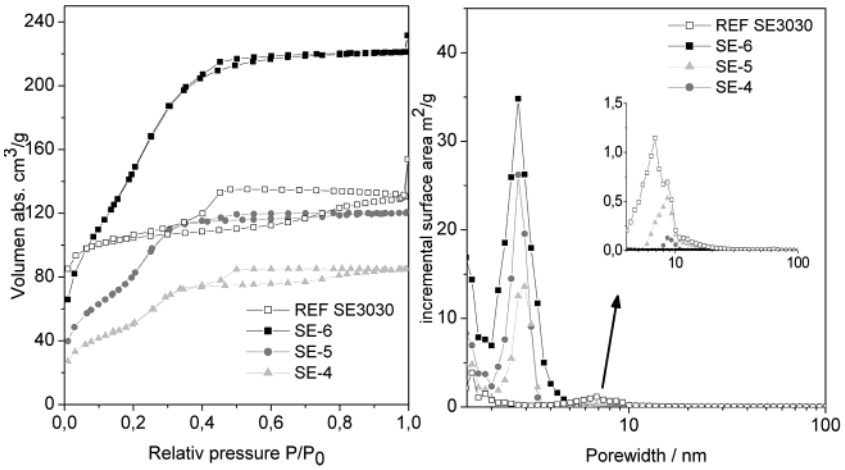

Figure 7. Isotherms of the materials SE-4 to SE-6. The shape of the isotherm is now dominated by the small pores formed by the OTN polymer. DFT calculations show clearly the shift of the SE pore distribution toward higher values, as compared to the SE pores in the materials SE-1 to SE-3 and the reference material.

Table 3. Surface and Overall Porosity of the Calcined Materials in Dependence on Added OTN Content

	SE3030	SE-1	SE-2	SE-3	SE-4	SE-5	SE-6
BET surface [m^2/g]	354	488	492	527	184	299	565
porosity [cm^3/g]	0.20	0.27	0.28	0.30	0.13	0.19	0.34

porosity is mainly seen in the range up to 0.3 relative pressure. The shape of the hysteresis loop changes only slightly and still exhibits type IV behavior, according to IUPAC nomenclature.

DFT calculations (Figure 6b) reveal this additional porosity to be similar to that of pure OTN phases, but the two types of pores cannot be deconvoluted. Just for SE-3, a distinct pore size starts to become visible. The corresponding BET surface areas are listed in Table 3. The expected linear increase of surface area from sample SE-1 to SE-3 goes well with the additional mesopore volume created by OTN micelles.

Obviously, up to this concentration, the two type of micelles stay separated but do form a common phase, with the smaller OTN micelles being embedded in the interstitial sites between the block copolymer micelles. To the best of our knowledge, this is the first manifestation of such a mixed micellar phase.

Both the BET surface area and the shape of the adsorption/desorption isotherms change dramatically with still increasing OTN content, as seen in Table 3 and shown in Figure 7. Despite the increased amount of template, the surface area and the overall porosity have decreased, speaking for the fact that parts of the surfactant are lost for the micellar casting. The DFT calculations show the dominance of the OTN pores but also the suppression of the SE3030 pores, the leftovers of which in addition exhibit an increased size.

Electron microscopy reveals the reason for these changes: the samples demix in two micellar phases. For SE-4, still mixed micellar regions are found, but the majority of the sample is demixed into fine, homomicellar regions (data not shown). For SE-5 (Figure 8a,b), the demixing is getting more pronounced, whereas the size of the demixing regions is largest for the SE-6, the sample with the highest fluorocarbon concentration (data not shown).

A careful observation of the pictures reveals the reason for the drop of surface area. In addition to the already mentioned incomplete access to the pore system of the pure OTN phase and the dispositional loss of surface area and porosity, the pore size of the SE structures has been significantly increased, partly to structures of up to 20 nm. Presumably, the two micellar phases compete for the

Table 4. Compositions of the Mixed Micellar KLE3935-Based Materials under Discussion

sample code	KLE3935/g	OTN/g	% template giving small pores	HCl, pH = 2/g	TMOS/g	SiO_2/g	wt % template in completely condensed material	carbon-free after calcination?
KLE-1	0.45	0.09	17	1.37	2.56	1	35	no
KLE-2	0.31	0.29	48	1.78	2.56	1	38	no
KLE-3	0.22	0.43	66	1.51	2.56	1	39	yes
KLE-4	0.14	0.55	80	1.81	2.56	1	41	yes
KLE-5	0.04	0.72	95	1.99	2.56	1	43	yes

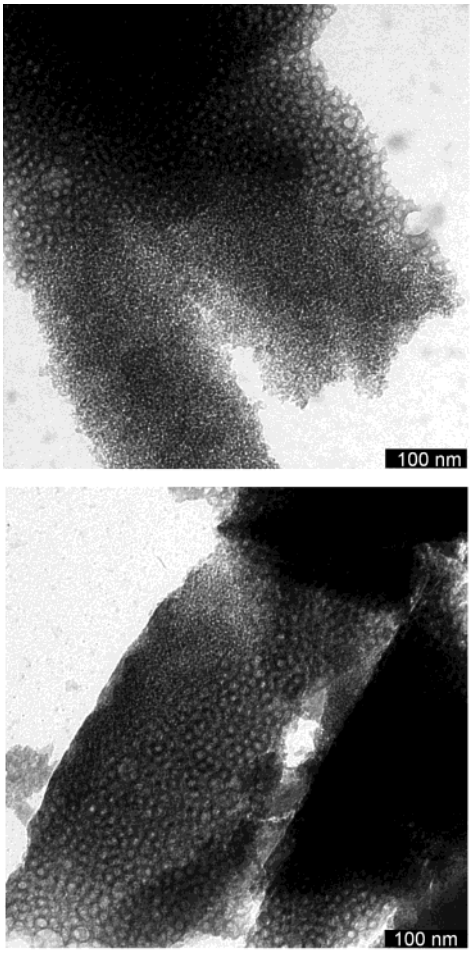

Figure 8. TEM of sample SE-5 showing only demixed regions of the two different pore systems.

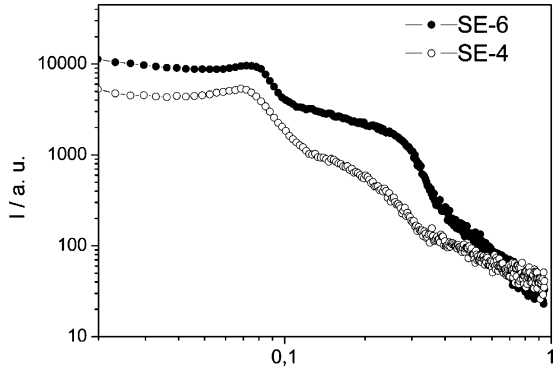

Figure 9. SAXS data of two different materials synthesized with SE3030 and OTN. The maximum of the scattering curve at low scattering values is a property of the SE pores, whereas the shoulder at higher scattering angles belongs to the pores generated by the fluorinated surfactant.

solvent, with the fluorinated micelles obviously having the higher osmotic pressure. Because of that, the SE3030 phase is higher in template concentration, and larger aggregates or even vesicular or droplet structures do form. Due to the difference in osmotic pressure, the coexistence with a mixed micellar phase is excluded. With increasing OTN content, the surface area is increasing again, however just based on the OTN-type pores. The phase boundary between one-phase and two-phase regions seems to be located at about 40 wt % OTN content with respect to the organic phase.

The advantage of nanocasting and the ability to depict the detailed phase structure is illustrated by comparing those results with the X-ray data of the calcined material. Figure 9 shows the SAXS data for two of the synthesized materials with different contents of OTN in the demixed region. The curve is essentially dominated by the form factor of the big pores, with some Percus−Yevick-like interference function at small angles due to the mutual packing. The richness of the structure or even the much weaker scattering due to the OTN structure however

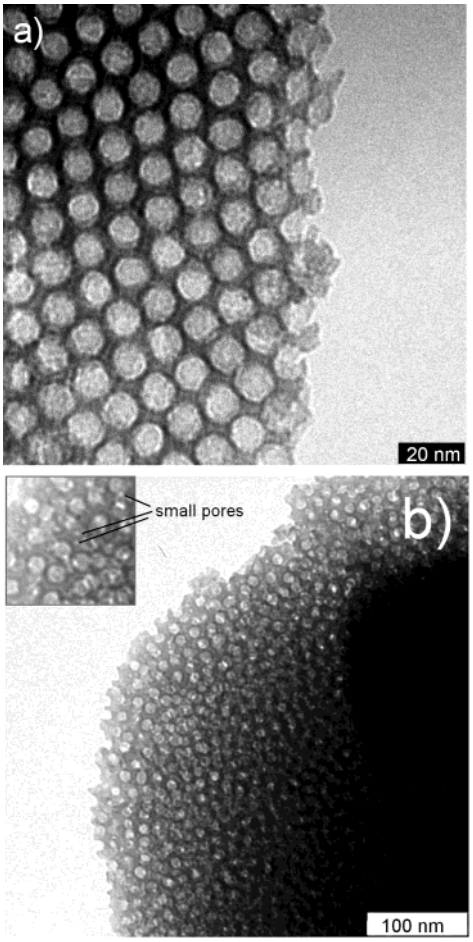

Figure 10. TEM pictures of samples KLE-1 (a) and KLE-2 (b). As the OTN content increases, the ordering of the sample decreases (b). For the sample KLE-2, the small pores generated by the OTN oligomer can be visualized between the KLE pores (see the inset).

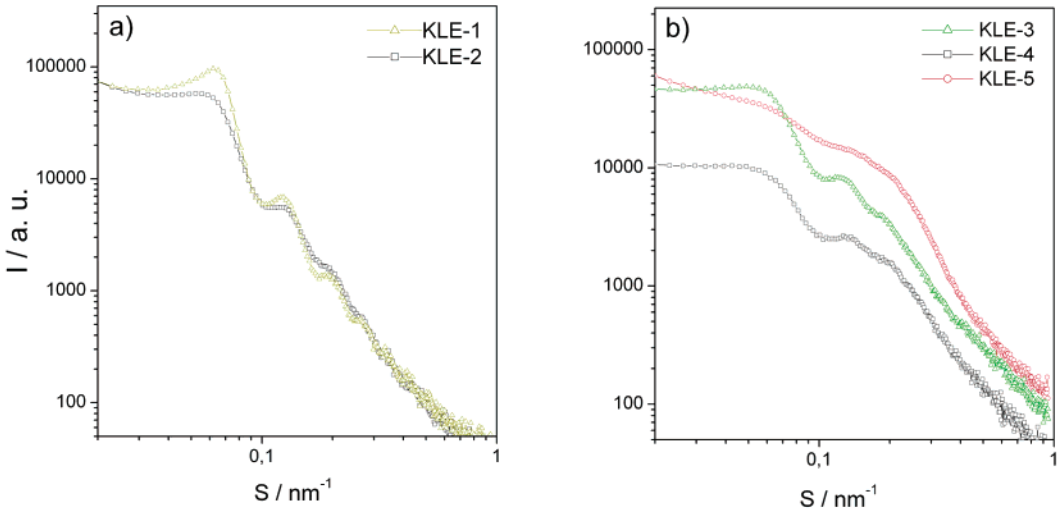

Figure 11. The SAXS curve of sample KLE-1 reflects the highly ordered fcc-type arrangement of the monodisperse pores generated by the template (a). With increasing content of OTN, the samples loses the order of the big pores, and a shoulder of the smaller pores due to OTN micelles at higher scattering values starts to grow (samples KLE-3 to KLE-5) (b).

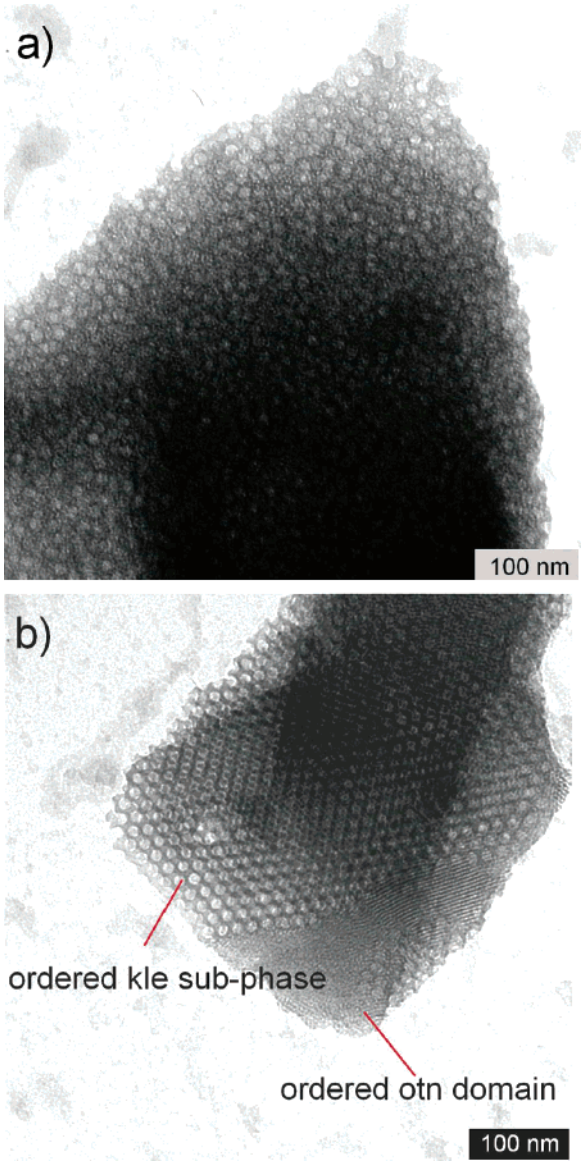

Figure 12. TEM characterization of sample KLE-3: (a) metastable homogeneous mixed micellar phase; (b) demixed double liquid crystalline phase.

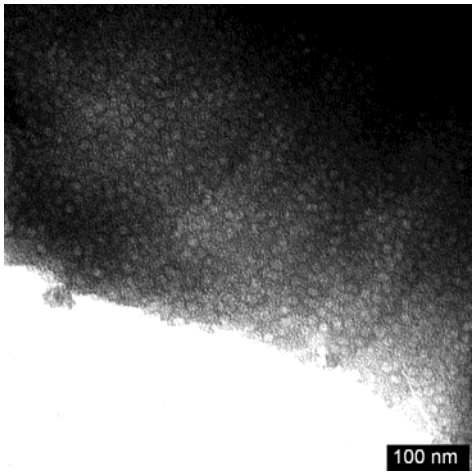

Figure 13. KLE-4 shows perfect miscibility of the two different micelles. The big pores generated by the KLE3935 micelles are statistically distributed in a matrix of the small micelles formed by OTN.

remains unseen. This is why SAXS cannot be employed to reveal quantitative information for this more complex system.

Nanocasting of the KLE3935/OTN System. As osmotic pressure around the micelle and size (because of depletion and packing effects) obviously play an important role for such micelle mixtures, system specificity is to be expected. Therefore, we applied this approach to a second nonionic fluorocarbon/hydrocarbon system, where OTN was mixed with KLE3935, a system forming regular spherical pores with 13 nm diameter with a strong tendency for cubic micellar packing.[4] Five porous silicas based upon OTN and KLE3935 with systematic variation of composition have been synthesized. The resulting compositions of the systems are summarized in Table 4.

For these systems, the compatibility between the two micellar species seems to be higher. For the samples with high hydrocarbon polymer micelle concentration, KLE-1 and KLE-2, respectively, almost clear KLE3935 behavior, only differing by the degree of order, is found. This is depicted in Figure 10.

The sample with the very low fluorosurfactant content is nicely ordered (face-centered cubic (fcc)), whereas

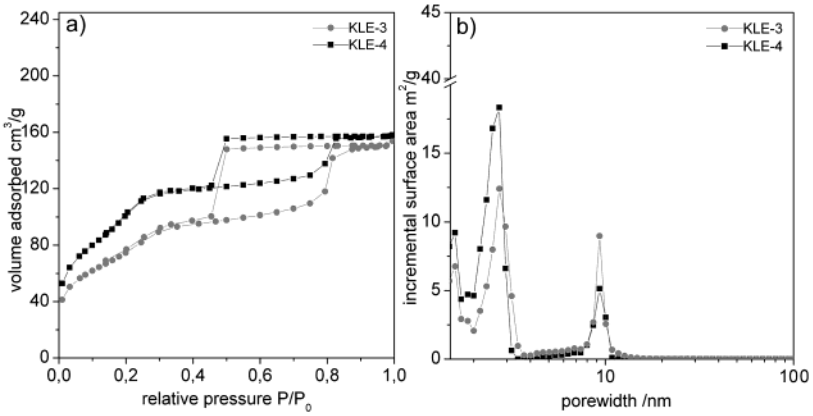

Figure 14. BET isotherms of samples KLE-3 and KLE-4. The relative amount of OTN and KLE3935 template, respectively, is reflected in the relative probabilities of finding the respective pore sizes in the DFT calculations.

increase of the content of fluoromicelles in the mixed micellar phase from 17% to 48% (relative to the total template) promotes disorder. The existence of pure OTN phases, which are usually quite easily identified (see the first set of experiments), can be denied on the basis of the TEM observations. Therefore, all the fluoromicelles must be located in the walls between the big pores, where TEM however can only give weak indications (see the zoom in Figure 10b).

Indirect evidence for this co-localization can also be taken from the fact that samples KLE-1 and KLE-2 were homogeneously black after calcination, whereas both pure reference materials with similar compositions would be certainly white. Obviously the presence of the fluorocarbon micelles in the regions between the block copolymer micelles suppresses percolation of the stabilizing PEO chains; that is, they are depleted onto the micellar cores. This assumption is supported by sorption measurements, which show no significant surface for both samples.

Also, the SAXS experiments go nicely with the TEM observations, as depicted in Figure 11a. In both cases, the scattering curves are dominated by the form factors due to the near monodisperse spherical pores, while the high fcc order of sample KLE-1 amplifies the maxima and minima of the curve.

For the sample with intermediary composition, KLE-3 (66 wt % fluorosurfactant of the total template content; note that the fluorosurfactant has a significantly higher density), an exciting metastability shows up. Depending on the fine details of preparation, either a stable mixed micellar phase (Figure 12a) or a mixture of the two pure liquid crystalline phases (Figure 12b) is obtained. This situation can be compared with the classical case of crystallization from an alloy: whereas the disordered phases are miscible, the crystalline phases are not, and demixing into microdomains of the pure compounds can take place. The fact that in the present case two liquid crystalline phases are concerned changes not the underlying physics but the time scale of metastability. This is an interesting model case of colloidal crystallization from the starting situation of a binary blend.

In contrast to the SE3030/OTN system, the KLE3935/OTN system is stable and miscible again at high OTN content. The TEM pictures of KLE-4 (Figure 13) and KLE-5 (not shown) show nicely the mixed micellar phases with two different pore sizes, where the abundance of each micelle type goes with the stoichiometry.

The presence of two different pore sizes is also clearly seen in the gas sorption measurements shown in Figure 14, where the results for samples KLE-3 and KLE-4 are shown. The two different regimes of sorption are also nicely separated by the DFT calculations revealing two distinct pore populations with incremental surface areas reflecting the stoichiometry. It must be underlined that the gas sorption of KLE-3 does not depend on the metastability of the sample structure, as the mixed micellar and the demixed double liquid crystalline state are practically indistinguishable in the gas sorption experiments.

Contrary to the SE system, the larger mesopores do not change their size even at very high OTN concentration, again underlining that this system is much better balanced with respect to mutual osmotic pressure.

The question is left of why the KLE3935 shows much better compatibility as compared to the SE system. If mixing were mainly entropic, the larger system would be less compatible, which is however not the case. Also, we do not observe any specific size effects, as they are found for metal alloys. We can only speculate that mutual recognition and acceptance of the micelles is due to the density of the nonionic PEO chains on both micelles and the coupled local osmotic pressures, which have to be balanced.

Conclusion

It was shown that micelles of fluorinated nonionic surfactants can be employed as templates in the nanocasting process to generate mesoporous silica. Depending on composition and the relative surfactant composition, highly organized hexagonal phases were identified with transmission electron microscopy. As fluorocarbons usually do not mix with hydrocarbons, those templates are also promising to promote the organization of hydrophobically modified monomer mixtures.

The mixture of those micelles with two amphiphilic hydrocarbon block copolymers allowed templating of silica with two independent, self-organized templates at the same time. The special feature of this fluorocarbon/hydrocarbon template mixture to form two individual micellar species under all conditions was confirmed: in not a single case did we find evidence for mutual structural cross-influence. By careful analysis of the pore architectures by gas sorption measurements and transmission electron microscopy of the final porous silica in dependence on the relative template concentration, parts of the phase diagrams could be revealed.

For the mixture between the polystyrene-*b*-poly(ethylene oxide), essentially macroscopically demixed samples, that is, the coexistence of two lyotropic phases, were found. Just in the case of high hydrocarbon and low fluorocarbon template content, a mixed micellar phase

was identified. This however turned out to be a closed pore structure: the coronas of the two micellar species do not percolate. In the coexistence region, the two lyotropic phases compete for the water, and the mesophase structure of the hydrocarbon block copolymer is altered by strong dehydration.

For the mixture between KLE3935 and OTN, miscibility over the whole composition space was identified. For high KLE contents, a mixed micellar phase where the two different micelles are packed in some type of organized alloy was identified. For all other compositions, the mutual presence lowers the order, and mixed micellar phases with liquid structure are observed. Close to symmetric composition, this liquid mixture can undergo "crystallization", and the coexistence of two highly organized liquid crystalline phases is clearly identified with the TEM experiments.

The nanocasting toward porous silica indeed serves in these experiments as an analytical tool, as such structural details of mixed micellar phases were previously not accessible. In addition, the obtained porous systems with controlled bimodal pore size distribution might be interesting from a materials perspective.

Acknowledgment. We thank the Clariant AG for providing us with the fluorinated surfactants. Steady support by the Max Planck Society is gratefully acknowledged.